Robotics and Computer-Integrated Manufacturing 41 (2016) 43–52

Contents lists available at ScienceDirect

Robotics and Computer-Integrated Manufacturing

journal homepage: www.elsevier.com/locate/rcim

Investigating the measurement of offshore wind turbine blades using coherent laser radar

Andrew Summers [a], Qing Wang [a,*], Neil Brady [b], Roger Holden [b]

[a] School of Engineering and Computing Sciences, Durham University, Durham DH1 3LE, UK
[b] Nikon Metrology UK Ltd., Staffordshire B77 5ES, UK

ARTICLE INFO

Article history:
Received 20 February 2015
Received in revised form
23 January 2016
Accepted 23 February 2016

Keywords:
Alignment
B-Spline
Coherent laser radar
Transformation
Unconstrained
Wind turbine blade

ABSTRACT

Large-scale offshore wind turbine blades need careful dimensional inspection at the production stage. This paper aims to establish an accurate measurement technique using Coherent Laser Radar technology combined with B-Spline point generation and alignment. Through varying the Degrees of Freedom (DoF), used for data point transformation, within the Spatial Analyser software package, erroneous inspection results generated by unconstrained blade flexing can be eradicated. The paper concludes that implementing a single B-Spline point generation and alignment method, whilst allowing transformation with DoF in *X*, *Y* and *Rz*, provides confidence to wind turbine blade manufacturers that inspection data is accurate. The experimental procedure described in this paper can also be applied to the precision inspection of other large-scale non-rigid, unconstrained objects.

1. Introduction

Large-scale offshore wind turbine blades have high geometric dimensional precision requirements which need to be inspected during the production stage to ensure designed geometrical tolerance specifications are satisfied. In the inspection procedure, aligning the computer-aided design (CAD) blade model to the measured blade data is integral to the measurement accuracy of the inspection. Minimising the measurement error during inspection, through robust data alignment techniques, provides blade manufacturers with confidence in their manufacturing procedures, enabling the design and build of more complex and aerodynamically efficient blade profiles [1].

With advances in manufacturing capability over past decades, the use and accuracy of metrology within the industry has increased dramatically. In recent years, particularly as computational technology has developed, metrology inspection is increasingly being used to optimise products at the design phase, thus enabling a better understanding of the product that is being manufactured.

In the case of large-scale wind turbine blade inspection, improved metrology technologies [2–5] enable manufacturers to make well informed decisions that are critical in creating superior blade prototypes [6].

There is a variety of metrology techniques that can be used to collect inspection data for wind turbine blades. These techniques require not only highly accurate large-scale measurement, but also the ability to transform, manipulate and align the measured data of this predominantly unconstrained object to a known reference frame, specified by a CAD model [7].

This requirement can be addressed in a variety of ways, depending on the unconstrained component's physical properties:

If a measured component is *not flexible*, a simple rigid transformation is enough to perform a data alignment between the CAD model and measured surface [8]. Rigid transformation, involving translation and rotation, is a simple and quick form of alignment.

If a measured component is *flexible*, it is necessary to use a more general transformation, such as the non-linear 'Iterative Closest Point' (ICP) method pioneered in [9]. This method works in six Degrees of Freedom (DoF) and accurately aligns data from unconstrained objects to their ideal geometric models established in CAD. The ICP method can also incorporate data point weighting and be combined with both rigid and non-linear transformation, as described in [10,11], to improve alignment accuracy, stability and convergence efficiency.

Another way of compensating for misalignment, due to flexing of the structural component, is demonstrated in [12]. Here, the Finite Element Method (FEM) is used to three dimensionally deform a non-rigid CAD model by the approximated component flex and then compare it with the measured state of the physically deformed component. This FEM approach has been proven to generate accurate representations of real deformations, however it

* Corresponding author.
E-mail addresses: andiesummers@hotmail.co.uk (A. Summers), qing.wang@durham.ac.uk (Q. Wang), neil.brady@nikon.com (N. Brady), roger.holden@nikon.com (R. Holden).

http://dx.doi.org/10.1016/j.rcim.2016.02.007

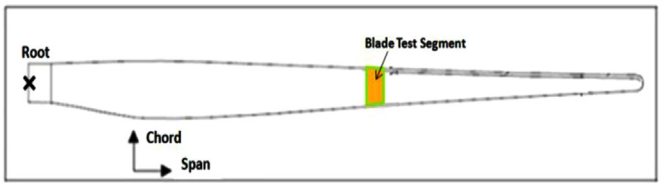

Fig. 1. The separation of a wind turbine blade CAD model into segments enabling independent measured and flex from the root to be eradicated.

is computationally expensive, slow and not always stable for large deformations.

With large-scale wind turbine blades subject to unconstrained flexing along the cord and span, these non-linear transformations or FEM methods could provide suitable alignment to ensure accurate metrology inspection during production of the entire blade.

More recently a relatively simple method has been developed by Nikon Metrology U.K. [13] and uses Coherent Laser Radar (LR) to measure independent segments of a complete blade. Through separating the measurement process of the blade in this manner, total blade flex can be compensated, allowing rigid five DoF transformations. This type of transformation as described in [14], enables accurate 'measured component to CAD' alignment. Once each segment of blade is measured and transformed, the data is then combined to form a complete blade representation (Fig. 1).

Although feasible, this procedure requires development and evaluation before implementation on industrial blade production lines. This paper, therefore, proposes an accurate, time efficient metrological data alignment transformation solution for large-scale wind turbine blades using LR technology. The solution will combat the erroneous data generated by flexing of wind turbine blades during inspection and provide blade manufacturers confidence in the accuracy of the data being fed back from the inspection procedure to the design stage.

This research develops and improves the Nikon Metrology measurement procedure currently implemented at the Vestas Winds Systems Research and Development facility on the Isle of Wight. It investigates, in detail, this inspection process and five DoF data alignment, where very little experimental evaluation has been carried out before, and gives clarity to the methods surrounding the inspection procedure used by wind turbine blade manufacturers.

2. Metrology theory

2.1. Various metrology techniques

There is a variety of metrology techniques that can be used to collect inspection data for wind turbine blades. These techniques digitise an object in one of two ways:

Contact Digitisation- A probe contacts a measurement surface and the *X*, *Y*, *Z* coordinate location is recorded. This is historically the highest precision form of measurement and is used widely in manufacturing inspection [15].

Non-Contact Digitisation- The contour data of the measurement surface is obtained through the use of vision technologies. There is zero contact force, thus preventing any deformation of the measurement surface. This method is favoured when measuring difficult to access surfaces quickly [16].

These contact and non-contact digitisation methods can be implemented independently or together, as shown in [17], and have metrological advantages and disadvantages.

For the inspection and quality checks of large-scale wind turbine blades during manufacture, non-contact Coherent Laser Radar (LR) is undoubtedly the most suitable metrology technology to use [18,19,20], as demonstrated in the metrology analysis [21,22] in Table 1.

Table 1
Analysis of metrology techniques against wind turbine blade inspection criteria.

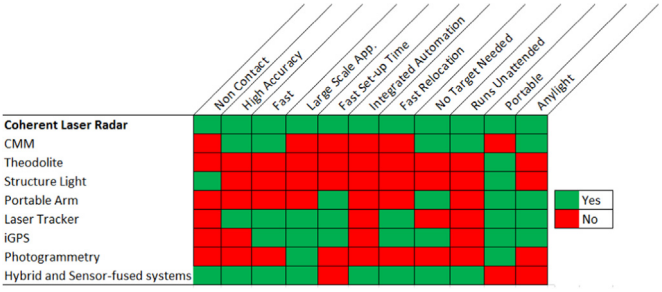

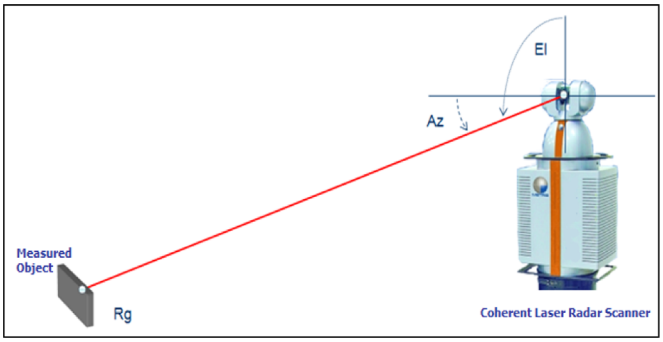

Fig. 2. LR scan mirror rotation and distance measurement.

2.2. Coherent laser radar technology and measurement

LR devices provide a robust and highly accurate form of measurement. They can capture complex, large-scale design model geometries to a high precision due to their large operating range and ability to work in any lighting condition [23]. The LR's set up is demonstrated in [20].

The LR can measure 48,000+ inspection locations with 0.025 mm single point uncertainty in an 8 h time period. The associated Spatial Analyser (SA) software collects the data and conducts CAD model comparisons to demonstrate manufacturing irregularities. The single point uncertainty for the measurement of a specific point in 3D space is highly dependent on the parameters range (*Rg*), azimuth (*Az*) and elevation (*El*). Through the finite accuracy of the angular measurement of *Az* and *El*, the contribution of *Az* and *El* to the single point uncertainty gets higher when the distance between laser radar scanner and measurement point gets higher.

The LR used in this investigation is Nikon Metrology's FM CLR Scanner (LR-200), a scanner that works with precise beam steering, delivered through a two axis gimble mounted scan mirror. The LR's measurement beam scans to a Range (*Rg*) of 50 m and is controlled through 360° in Azimuth (*Az*) and 120° Elevation (*El*) (Fig. 2).

The LR calculates range by bouncing a laser beam, generated by the instrument, off the object being measured and then compares the frequency signal of reflected laser beam light to an internally generated and calibrated duplicate frequency signal. The difference in light beam frequencies (Δf), as shown in Fig. 3, is used to calculate range accurately to within 10 μm [23], using Eq. (1).

$$Rg = \Delta f / 0.667 \quad (in\ microns) \tag{1}$$

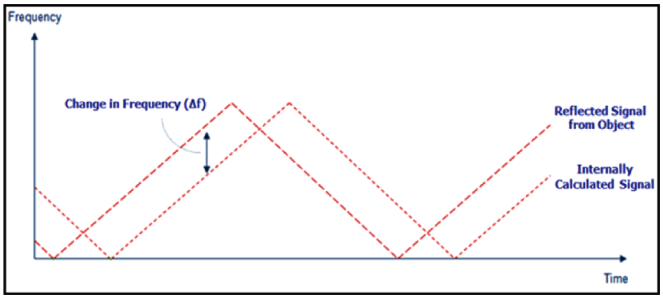

Fig. 3. The saw tooth wave of base frequency200 THz that enables Δf to be calculated due to a fixed wavelength of 1500 nm.

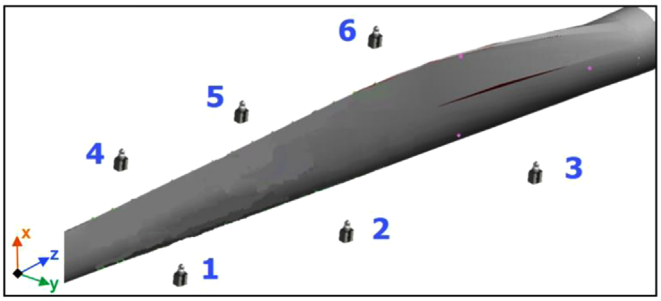

Fig. 4. Inspection locations required for complete inspection of a 60 m blade using LR.

Combining this range with the Azimuth and Elevation angles locates the point measured on the object. This measured point is then converted into a Cartesian coordinated system by the LR operating software SA [25] and displayed in the user interface.

LR measurement requires 'line of sight' to record the orientation of measured points, requiring multiple instrument locations (as shown in Fig. 4) when inspecting complete, large-scale objects. Current blade inspection methods, [13], have shown that six instrument locations are required to record a complete 60 m wind turbine blade. This causes additional orientation problems for the SA operating systems to overcome.

2.3. Spatial analyzer: errors and uncertainty

SA is a flexible, instrument independent and traceable 3-D graphical software package that provides a platform for component inspection and data analysis.

When using SA in conjunction with LR, the software is particularly capable at accommodating multiple instrument locations through its Unified Spatial Metrology Network (USMN) programme [26]. This programme is based on the Guide to the Expression of Uncertainty in Measurement (GUM) approach [27–29] and converts each data set collected at each instrument position into one unified coordinate orientation, whilst minimising error and quantifying the uncertainty associated with data transfer from the LR to the software system [30]. This makes SA a powerful tool and reduces the impact of the error multiplying effect caused by the large-scale measurement.

Once this data collation is completed, SA enables the entire measured component to be analysed against its design CAD drawing to ensure a high quality of manufacture.

By way of comparison, rather than using a single LR metrology instrument, research has also been conducted into combining metrology techniques to achieve the accurate measurement of freeform objects [31].

Fu et al. [17] considers the use of two different instruments to measure complex freeform surfaces. Using a non-contact Structured Light optical scanner and a contact measurement coordinate-measuring machine (CMM), the authors highlight the difficulties that arise with error evaluation. Particular problems occur with the CAD model and point cloud data generated from the optical scanner being impossible to automatically align, making the approach time consuming and inaccurate. The paper also explores new ways of detecting digital error and uses the 'golden section method' to reduce position errors in alignment caused by inconsistency between actual references and CAD model references. The added complexity associated with using multiple metrology technologies reinforces the advantages of the simple operation of LR.

2.4. B-splines points

To measure a manufactured turbine blade's aerofoil profile successfully and then compare this data to the required shape in the form of a CAD model, the data must be unified in the same coordinate system. This alignment is achieved through the construction of data points along the CAD model's surfaces.

To generate the required data points within SA, 'B-Spline' curves are constructed following the complex curved surface profiles of the CAD blade [31,32]-the curves then provide the location framework for the points. B-Spline curves are normal to the span of the blade and their frequency can be varied, depending on the level of inspection detail required (Fig. 5).

A B-Spline Curve, $P(t)$, is formulated using the de Boor algorithm [33], with control points, P_i, and k being the order of polynomial segments.

$$P(t) = \sum_{i=0}^{h} P_i N_{i,k}(t) \tag{2}$$

Once the de Boor algorithm, shown in Eq. (2), is used to construct a B-Spline curve in SA, points are constructed at even distances along this B-Spline curve. The points positioned along the analytically defined B-Spline curve then require projecting to the CAD model's geometrically defined curve. Doing so, removes the error caused by the B-Splines multiple straight line construction, shown in Fig. 6.

B-Spline projected points along the CAD surface provide the reference locations within the SA coordinate system to which measured points are aligned. Kumar et al. [34] states that B-Spline curves are a reliable form of surface fitting points whilst de Boor [35] shows they provide a flexible and useful tool for the computer interpolation.

2.5. Data alignment

In order for alignment within SA using LR, the blade CAD model is separated into multiple segments. For each of these segments, B-Splines points are generated around the blade chord to form a framework for measurement and alignment, as shown in Fig. 5.

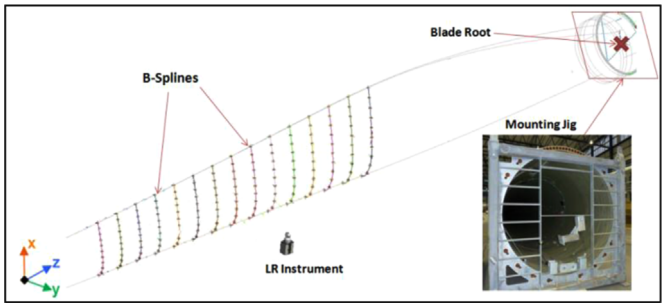

Fig. 5. B-Spline generation about the blade chord and the *Z*-axis constraining mounting jig.

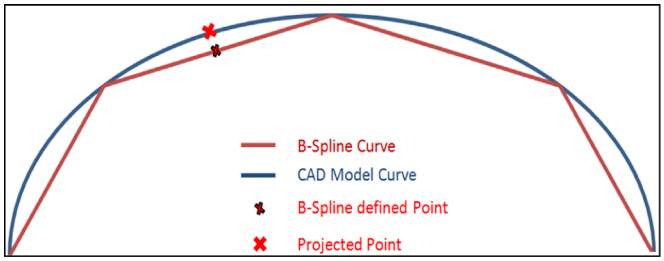

Fig. 6. Illustration of the point location error caused by the difference in CAD model surface curve and B-Spline construction.

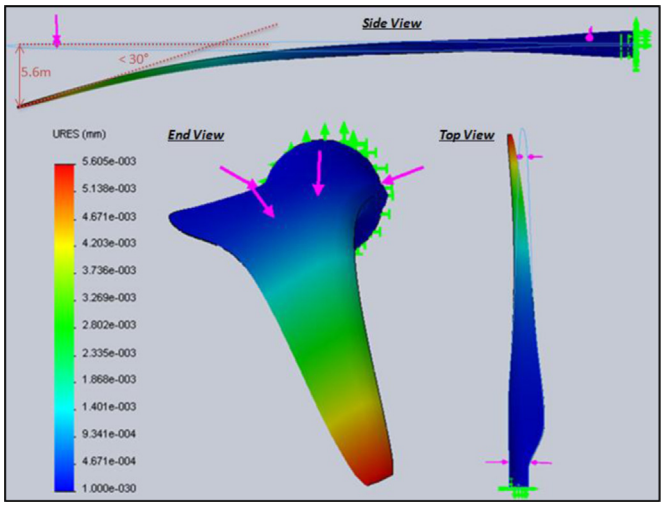

Fig. 7. SolidWorks flex of blade analysis.

Once measured, the B-Spline points are aligned with SA. Due to wind turbine blades being constrained at the root by their inspection mounting jig in the *Z*-axis, SA alignment involves five DoF transformations in *X*, *Y*, *Rx*, *Ry* and *Rz*. Any combination of these five DoF transformations can be used to achieve the optimum (best) data alignment. Having five variables gives $2^5=32$ different DoF combinations and through quantifying and analysing all 32 variations, the optimum DoF transformation combination can be established.

This optimal alignment is defined as the 'minimum offset of the B-Spline points within the CAD coordinate system to the measured points coordinate system' and when completed provides an accurate comparison between measured blade profile and blade CAD model profile. Combining these profiles for each segment together builds a picture of the entire blade manufacturing accuracy.

2.6. Blade flexing

To establish the flex characteristics of a large-scale wind turbine blade, the displacement of the blade from its rigid position and the angles at which it moves away from this position can be calculated using Computational Analysis.

These values are important as they help define the maximum coordinate system offset (sag and twist), caused by gravity, experienced during wind turbine blade inspection. The data is used to justify the magnitude of the experimental flex simulations imposed on the test piece described later in this paper.

The Computational Analysis in this work used SolidWorks and a 44 m long Vestas Blade CAD model to estimate the maximum angle and maximum displacement to which a large-scale wind turbine blade could be exposed. Fig. 7 shows the effect of applying a uniform force, simulating the effect of gravity, to the upper surface of the profile whilst constraining the CAD blade at the root. This simulates the blade flex during inspection.

The results of this total blade analysis shows that acting like a cantilever, the blade flexes (sags) with maximum displacement of 5.6005 m from its original, rigid position, enabling the maximum angle change induced by this displacement to be calculated as a maximum of 30° from the *Z*-axis running along the blade span.

This analysis provides the maximum values of flex experienced by the blade and represents the worst case scenario that could occur in a factory inspection procedure. In practice, the blade is mounted trailing edge up with a trolley positioned under the leading edge. This causes only a small rotational flexing about *Rx*, *Ry* and *Rz* rather than the extreme flexing demonstrated by the SolidWorks flex simulation.

Achieving optimised accuracy for the worst case state will ensure that the smaller magnitude alignments experienced in day-to-day measurement of the blades at the factory can be confidently proposed as the most accurate method.

2.7. Enhanced surface point measurement

In order to generate the results, the LR approach offers both Regular and Enhanced Surface Point measurement. The latter process takes multiple measurements surrounding the selected Azimuth and Elevation position in order to return the best result, whilst the regular measurement process returns only one measurement for the specific location of the laser beam (Fig. 8).

The Regular method causes greater irregularities and errors than the Enhanced method as demonstrated from running a back-to-back LR comparison experiment: This experiment involved generating, through using SA, a straight line along a flat surface. Along this line, 250 nominal points were constructed and each of these measured by the LR in both Regular and Enhanced Surface Point measurement configuration. The distance between the laser radar and cross section of the model is 5.5 m.

Comparing the measured results with the nominal points generated in SA along the line quantifies the difference between the two methods. The results were:

Regular Surface Point measurement:
Max Displacement from straight line = 0.9 mm
Mean Variance = 0.3 mm
Enhanced Surface Point measurement:
Max Displacement from straight line = 0.1 mm
Mean Variance = 0.01 mm

These results show that for consistency and accuracy of measurement the Enhanced Surface Point measurement is best. The Mean Variance of 0.01 mm also justifies the use of an error range of ± 0.01 mm when analysing data generated by the LR. The downside to this is extended measurement time; however, this is not a concern for this experimental application.

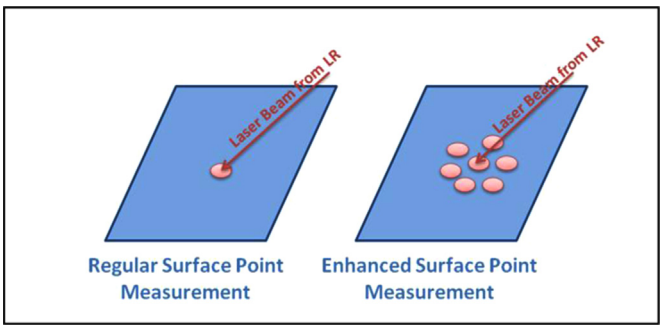

Fig. 8. Comparison between Regular and Enhance Surface Point Measurement procedure.

3. Measurement method

Incorporating the theory discussed above, the method used to investigate and optimise large-scale wind turbine blade inspection was established.

3.1. Test piece design

To carry out laboratory experimentation using the LR, a plywood test piece was designed with a curved measurement surface, loosely based around the Vestas blade test piece. Mounted on a gimble (allowing *Rx* and *Rz*) and turntable (allowing Ry), the test piece is designed to simulate large-scale wind turbine blade flexing within a laboratory environment whilst eradicating the disadvantages of the Vestas supplied test piece, which were:

- Too large and heavy for the Durham University metrology laboratory.
- Inaccurate control of rotation through *X*, *Y*, and *Z*-Axis (*Rx*, *Ry* and *Rz*).

The newly designed test piece improved on these aspects with a smaller, lighter and more easily movable construction.

The turntable and gimble enable controlled rotation to within 1° accuracy, simulating blade sag in Ry (up to 30°) and blade twist in *Rx* (up to 15°) and Rz (up to 20°). They also prevent the test piece moving along the *Z*-axis. The *Rx*, *Ry* and *Rz* offsets replicate the blades flex characteristics and constraints demonstrated in the SolidWorks simulation in Fig. 7.

The test piece was constructed to accurately match a CAD model, also used for alignment and comparison in SA, and is 1.5 m high. Its shape imitates a simplified blade profile and represents a small segment of an entire blade at a position 30 m from its root. Fig. 9

3.2. Test piece evaluation

To generate accurate comparative data between SA generated B-Spline points based on a CAD model, and measurement points on the test piece, consistency between the manufactured test piece and its CAD model is vitally important.

To double check this dimensional accuracy, the complete test piece was measured with the LR. The results showed that at four equally spaced locations across the measurement surface, the average dimensional differences between the CAD model and test piece were 0.013 mm, 0.011 mm, 0.005 mm and 0.007 mm (mean = 0.009 mm).

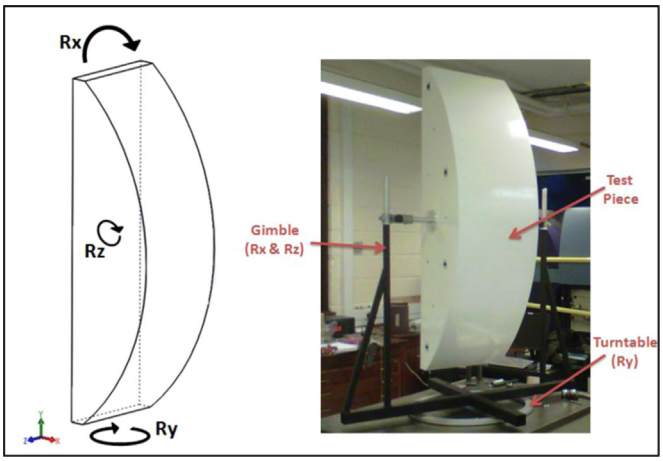

Fig. 9. Left, the CAD model of the test piece with rotational DoF marked. Right, the test piece within the laboratory.

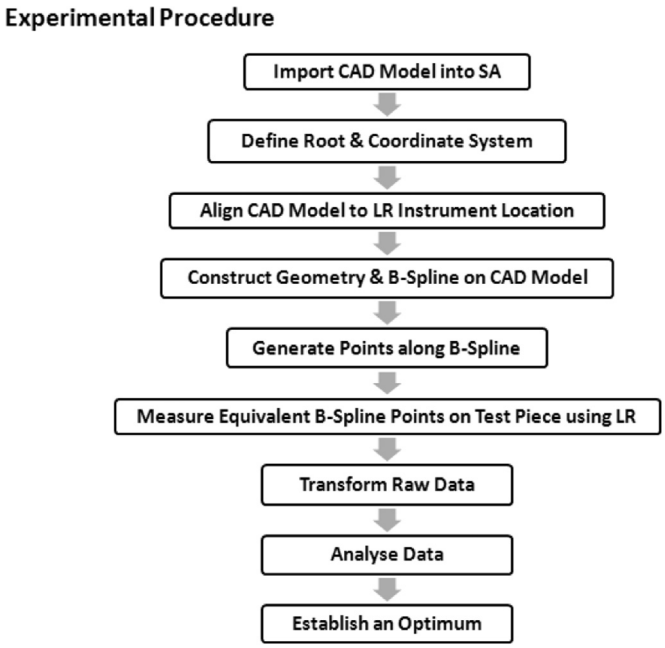

Fig. 10. Blade test experimental procedure.

This provides strong evidence that the test piece will not generate artificial results due to an inaccuracy of CAD to test piece dimensions.

3.3. Test piece measurement

The test piece was measured using the LR on its curved, constant radius surface designed to represent a simplified blade aerofoil outer surface. The LR was positioned 4 m from the test piece, which was mounted 1.5 m from the laboratory floor. Throughout the experimental procedure, a clear 'line of sight' was left between the LR and test piece with the LR never being moved.

3.4. Experimental procedure and data transformation

The experimental procedure is designed to establish a quick, simple and accurate way of measuring large-scale wind turbine blades. Each experiment carried out followed the systematic procedure framework as shown in Fig. 10. This framework also forms the basis for the complete inspection procedure proposed for future industrial implementation.

Carried out in a controlled environment, this experimental procedure (Fig. 11) enables a full 32 DoF combination analysis to be conducted within the data transformation stage.

This thorough but time consuming full enumeration enables each variation of DoF constraints for example, *Z* constrained and *X*, *Y*, *Rx*, *Ry*, *Rz* unconstrained, to be applied in order to evaluate the optimal transformation constraints.

Another benefit of this systematic procedure is that it enables different geometries and numbers of B-Spline curves to be evaluated reliably without changing other aspects of the process.

A combination of these two experiment variations (DoF and B-Spline geometries/number) form the final optimised system, demonstrating the most robust procedure to ensure measured data is represented accurately during blade inspection.

3.5. Experimental plan and objectives

Having designed and constructed the test piece, conducted initial experimentation to validate the accuracy of the test piece and developed the experimental procedure, the investigation

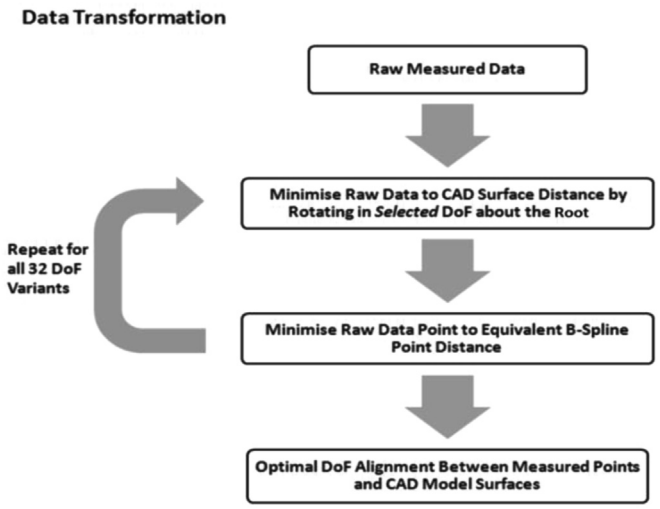

Fig. 11. Blade test data transformation procedure.

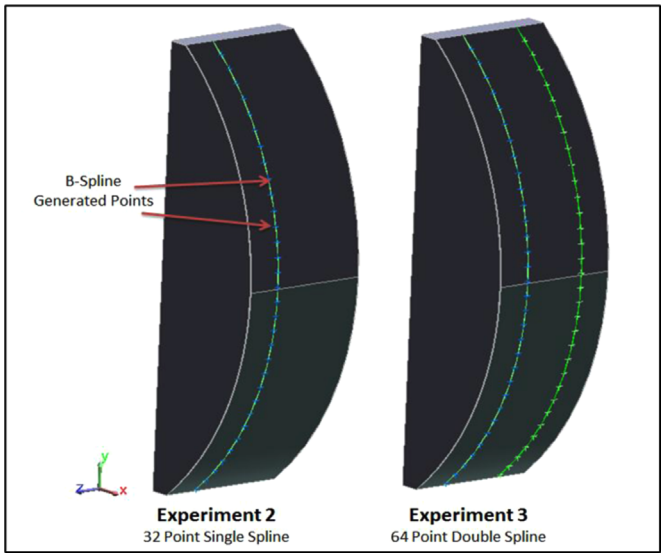

Fig. 12. Experiment 2 and Experiment 3 B-Splines points, generated within SA.

experiments were established as:

Experiment 1. Vary distance of the root along the constrained *Z*-axis of a wind turbine blade.

This experiment establishes whether the position of a blade inspection segment along the blade affects the data alignment accuracy.

Experiment 2. Conduct a full 32 DoF combination evaluation with a single B-Spline curve whilst simulating blade flex in *Rx*, *Ry*, and *Rz*.

This establishes a DoF combination that optimises alignment accuracy when measuring 32 points along a single B-Spline curve (Fig. 12).

Note that the selection of 32 measuring points has no linkage to the 32 DoF possible combinations – the numbers are coincidental.

Experiment 3. Conduct a full 32 DoF combination evaluation with double B-Spline curves whilst simulating blade flex in Rx, Ry, and Rz.

This establishes a DoF combination that optimises alignment accuracy when measuring two combined 32 point B-Spline curves.

Experiment 4. Using the optimised DoF combinations from Experiment 3, evaluate the effect that changing the B-Spline curve separation has on quality of results.

This establishes if changing the distance between B-Spline curves can achieve a superior solution than experiment 2 or 3.

These four experiments were conducted following the procedure previously shown and used 32 B-Spline points constructed 50 mm apart.

3.6. Data collection and analysis criteria

After conducting each experiment, the data is displayed in SA in the form of:

Vector Magnitudes-illustrating the distance between the 32 measured points and the CAD model surfaces.
Mean Point-to-Point Distance-illustrating the mean distance between the 32 measured points and the 32 equivalent B-Spline generated points.
Instrument Movement – illustrating the amount the LR instrument has notionally moved from its original position within SA to achieve the transformation.
The data is then analysed with the optimal DoF combination for each experiment. This requires:
Smallest Standard Deviation of Vector Magnitudes – generated from the mean of all vector magnitudes, the standard deviation must be minimised in order to demonstrate that the measurement points have been successfully aligned with the CAD model surface.
Smallest Mean Point-to-Point Distance – minimising this distance shows that the data measured and collected is representative and aligned to a specific CAD model feature.
Smallest Instrument Movement – to ensure errors are minimised when physically changing the LR instrument location for complete blade inspection, any notional movement of the LR instrument within SA must be minimised.

3.7. Ranking

In order to establish a hierarchy of results, the three forms of analysis, mentioned above, provide independent factors to which each DoF combination is ranked from 1 to 32, with the most accurate DoF combination assigned a Rank Score of 1. For each experiment conducted, the three independent factor rank scores are then summed to form the overall Total Rank Score (Fig. 13) achieved by each DoF combination. Weighting is not assigned to any of the factors, as each factor has equal analytical importance.

The DoF combination that achieves the smallest Total Rank Score for the experiment is then (realistically) assumed to be the most accurate form of measurement alignment. Comparing Total Rank Scores across experiments will identify any reoccurring, strong performing DoF combinations.

However, if all results from an experiment have high Total Rank Scores, this highlights that all DoF combinations are performing poorly or inconsistently against the analytical criteria and therefore no accurate data alignment can be established.

Ranking results with particular relevance are those from Experiment 2.4 and 3.4 (see below), which simulate Rx, Ry and Rz movement similar to that experienced by wind turbine blades in a factory inspection procedure.

Once the ranking has identified optimal alignment methods for both single and double B-Spline curves, the data sets are compared to establish the superior approach.

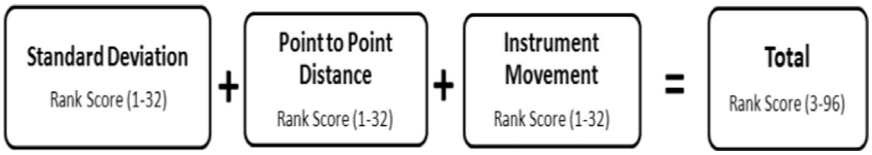

Fig. 13. Establish of total rank score.

3.8. Transformation movement percentage

In order to quantify the 'movement' from unaligned to aligned measured data points, caused by the transformation, the vector magnitudes from the CAD model surface to the measured data points before the alignment and after the alignment are calculated. The range of each of these aligned and unaligned vector magnitudes then enables the Transformation Movement Percentage (TMP) to be calculated using Eq. (3).

$$\text{Transformation Movement Percentage} = \left(1 - \frac{\text{Aligned Vector Magnitude Range}}{\text{Unaligned Vector Magnitude Range}}\right) \times 100 \quad (3)$$

The TMP, when combined with the Total Rank Scores, establishes the overall most accurate DoF combination for data point transformation.

4. Results and analysis

All results are measured in millimetres (mm) and rounded to the nearest 0.01 mm due to the precision of the Enhance Surface Point Measurement procedure implemented.

4.1. Experiment 1

This experiment evaluated if changing the position of the root from 1 m to 50 m along the *Z*-axis within SA affects the alignment accuracy. It was conducted using single B-Spline point generation, a 10° Rz test piece offset, and took measurements for a variety of DoF combinations.

Through comparing the 1 m root and 50 m root results, the maximum variation of the three analytical factors is ± 0.01 mm. This illustrates that the position of the root along the constrained *Z*-axis does not affect alignment performance or accuracy.

4.2. Experiment 2

Experiment 2 identifies the optimal DoF combinations when applying a single B-Spline point alignment technique to various test pieces offset scenarios.

Experiment 2.1: A 30°Ry test piece offset, simulating the maximum sag along an unsupported blade span.

Table 2 identifies that the constrained DoF combination of *Z*, *Rx* and *Ry* produces the lowest Total Rank Score of all the 32 DoF combinations investigated. Constrained Z, *Rx* and *Ry* DoF also generates the highest TMP of 94% and therefore indicates this DoF combination has the best overall data alignment performance when compensating for Ry misalignment caused by blade sag.

Experiment 2.2: A 10° Rz test piece offset, simulating the maximum twisting about the blade cord's Z-axis.

Table 3 identifies that to compensate for misalignment caused by blade twist about *Rz*, constraining the *Z*, *Rx* and *Ry*, again, produces a strong alignment performance-only additionally constraining the *X* DoF improves alignment performance marginally.

Experiment 2.3: A 30° Ry and 10° Rz test piece offset, simulating blade twisting and blade sagging.

Table 4, again, identifies that constraining the *Z*, *Rx* and *Ry* produces the most effective alignment of data compensating for blade sags and twists in the Rz.

Experiment 2.4: A 5° Rx, 30° Ry and 10° Rz test piece offset, simulating the most extreme scenario requiring data alignment.

Table 5 consolidates all results from Experiment 2, showing that when using single B-Spline point alignment to compensate for blade sag (Ry) and twist (Rx and Rz), the overall highest ranked transformation DoF are *X*, *Y* and *Rz* whilst keeping *Z*, *Rx* and *Ry* constrained.

The raw data and SA alignment performance vector magnitudes, for constrained *Z*, *Rx* and *Ry* DoF in *Experiment 2.4* (simulating the most likely configuration in a factory), are shown in Fig. 14. This DoF combination generates a 94% TMP from the unaligned, original

Table 2
Top 10 ranked results for experiment 2.1.

Rank	Constrained DoF	Total Rank Score	Transformation Movement (%)
1	*Z Rx Ry*	10	94
2	*X Y Z*	19	94
2	*X Z*	19	94
2	*Y Z*	19	94
2	*Z*	19	94
6	*X Y Z Ry*	29	94
7	*X Z Rx*	30	94
7	*Z Rx*	30	94
7	*X Z Rx Ry*	32	94
10	*X Y Z Rx Ry Rz*	34	79

Table 3
Top 10 ranked results for experiment 2.2.

Rank	Constrained DoF	Total rank score	Transformation movement (%)
1	X Z Rx Ry	4	95
2	Z Rx Ry	5	95
3	Z Ry	8	95
4	Y *Z Ry*	10	95
5	*X Y Z*	11	95
5	*X Z*	11	95
5	*Y Z*	11	95
5	*Z*	11	95
9	*X Y Z Ry*	27	95
10	*X Z Rx*	31	95

Table 4
Top 10 ranked results for experiment 2.3.

Rank	Constrained DoF	Total rank score	Transformation Movement (%)
1	Z Rx Ry	5	96
2	X Y Z	9	96
2	X Z	9	96
2	Y Z	9	96
2	Z	9	96
6	X Z Ry	26	96
7	Y Z Ry	28	96
8	Z Ry	29	96
9	X Z Rx	32	96
9	Z Rx	32	96

Table 5
Top 10 ranked results for experiment 2.4.

Rank	Constrained DoF	Total rank score	Transformation movement (%)
1	*Z Rx Ry*	4	94
2	*X Z Ry*	12	94
3	*X Y Z Ry*	23	93
4	*X Z Rx Ry*	26	91
4	*X Y Z*	26	94
4	*X Z*	26	94
4	*Y Z*	26	94
4	*Z*	26	94
9	*Y Z Ry*	30	94
10	*Z Ry*	31	94

measurement data and has strong performance with no notional instrument movement within SA, minimised Standard Deviation (1.39 mm) and minimised Mean Point-to-Point Distance (4.93 mm).

4.3. Experiment 3

Experiment 3 identifies the optimal DoF combinations that can be applied when using a 200 mm separation, double B-Spline point alignment technique.

Experiment 3.1: A 30° Ry test piece offset, simulating the maximum sag along an unsupported blade span.

Table 6 identifies a variety of DoF combinations that all exhibit the strongest alignment performance to compensate for blade sag. These, however, have high Total Rank Scores in comparison to equivalent results generated in Experiment 2. This is due to each of the DoF combinations performing inconsistently against the analysis criteria. In this case, the constrained DoF combinations with the lowest ranked scores of 16, compared with 10 in Experiment 2.1, have low Standard Deviations of 4.11 mm and Mean Point-to-Point distances of 7.69 mm, but perform poorly due to notional instrument movement within SA. Therefore, these results do not provide a clear optimal alignment DoF combination.

Experiment 3.2: A 10° Rz test piece offset, simulating the maximum twisting about the blade cord's Z-axis.

To remove the effect of twist (Rz), Table 7, similarly to Table 6, does not show a clear optimal alignment DoF combination. Again, this is due to notional movement of the instrument within SA.

Experiment 3.3: A 30° Ry and 10° Rz test piece offset, simulating blade twisting and blade sagging.

Table 8 shows high Total Rank Scores, illustrating that the double B-Spline point alignment is performing inconsistently against the analytical criteria and not effectively compensating for the effects of both blade sag and twist.

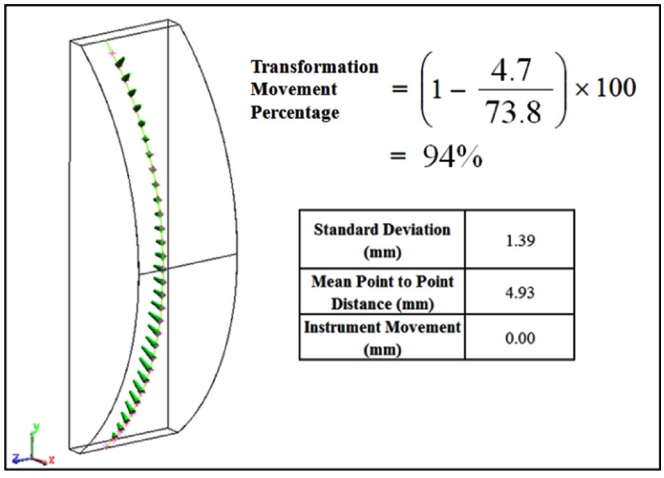

Fig. 14. Optimum Experiment 2 alignment accuracy results. Shown in SA *(left)*, the Transformation Movement Percentage and in performance raw data form *(right)*.

Table 6
Top 10 ranked results for experiment 3.1.

Rank	Constrained DoF	Total Rank Score	Transformation Movement (%)
1	X Y Z Rx	16	91
1	X Z Rx	16	91
1	Y Z Rx Ry	16	91
1	Z Rx Ry	16	91
5	X Y Z Rz	23	91
5	X Z Rx Rz	23	91
5	X Z Rz	23	91
5	Y Z Ry	23	91
5	Y Z Ry Rz	23	91
5	Z Rx Ry Rz	23	91

Table 7
Top 10 ranked results for experiment 3.2.

Rank	Constrained DoF	Total rank score	Transformation movement (%)
1	*X Y Z Rx*	10	89
1	*X Y Z Rx Rz*	10	89
1	X Y Z Rz	10	89
1	X Z Rx	10	89
1	*X Z Rx Rz*	10	89
1	*X Z Rz*	10	89
1	*Y Z* Rx Ry	10	89
1	*Y Z Rx Ry Rz*	10	89
1	*Y Z Ry Rz*	10	89
1	*Z Rx Ry*	10	89

Experiment 3.4: A 5° Rx, 30° Ry and 10° Rz test piece offset, simulating the most extreme scenario requiring data alignment.

In contrast to Experiments 3.1, 3.2 and 3.3, allowing rotational DoF in Experiment 3.4 removes notional LR instrument movement. This causes the results in Table 9 to show strong performing alignments without the high Total Rank Scores previously observed. This contrast further highlights the inconsistencies of establishing an optimal DoF combination when subjecting 200mm separation double B-Spline point alignment to different test piece offsets.

However, to conduct comparative analysis with Experiment 2, the raw data and SA alignment performance vector magnitudes from the optimal DoF combinations, established in *Experiment 3.4,* are used. These results, as shown in Fig. 15, use *X* and *Z*, or *Z* (both the same) constrained DoF combinations and have a TMP of 93% from the unaligned data. These results show a low Standard Deviation of 1.64 mm, a low Mean Point-to-Point Distance of 5.07 mm and no notional Instrument movement within SA.

Table 8
Top 10 ranked results for experiment 3.3.

Rank	Constrained DoF	Total rank score	Transformation movement (%)
1	*X Z Rx*	29	95
1	*Z Rx Ry*	29	95
3	*Y Z Ry*	36	95
3	*Y Z Ry Rz*	36	23
5	*X Y Z*	37	95
5	*X Y Z Rz*	37	23
7	*X Y Z Ry*	39	23
7	*X Z Rx Rz*	39	84
7	*Z Rx Ry Rz*	39	23
10	*Y Z Rx*	43	23

Table 9
Top 10 ranked results for experiment 3.4.

Rank	Constrained DoF	Total rank score	Transformation movement (%)
1	*X Z*	3	93
1	*Z*	3	93
3	*X Y Z*	4	93
3	*Y Z*	4	93
5	*Z Ry Rz*	24	42
6	*Z Ry*	25	42
7	*X Z Rx*	33	93
7	*Z Rz*	33	42
9	*X Z Rz*	35	42
10	*Y Z Rz*	36	42

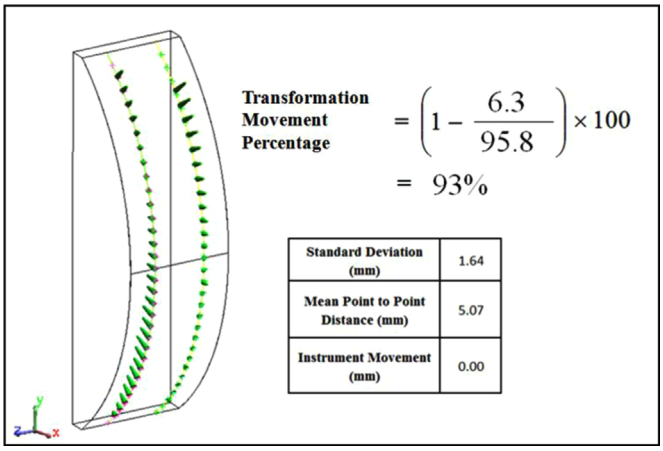

Fig. 15. Optimum Experiment 3 alignment accuracy results. Shown in SA *(left)*, the Alignment Improvement Percentage and in performance raw data form *(right)*.

4.4. Experiment 4

Experiment 4 results show that by reducing the separation distance between double B-Splines curves from 200 mm to 50 mm, the TMP moves marginally from 93% to 94%, however the inconsistencies illustrated by the results of Experiment 3 remain.

5. Discussion

5.1. Single B-spline point alignment

The analysis for single B-Spline point alignment shows that as the number of constrained DoF increases, the ability of SA to align the measured data points becomes limited. This causes an overall trend of poor alignment transformation performance, demonstrated by larger Standard Deviations of the measured points to the CAD surface vector magnitudes (23.21 mm for constrained *X*, *Y*, *Z*, *Rx*, *Ry* and *Rz*), and a larger Point-to-Point distance (20.72 mm for constrained *X*, *Y*, *Z*, *Rx*, *Ry* and *Rz*). Despite this, as DoF constraints increase, the overall notional LR instrument movement within SA reduces, indicating strong performance relating to this analysis criteria.

This result means that an optimum DoF combination for single B-Spline point alignment must either be a compromise between these three analysis criteria trends or a combination of constrained DoF that have no effect on the ability of SA to transform the data points.

In the latter case, the results ranking system and TMP calculation have highlighted that the constrained DoF combination of Z, Rx and Ry enables SA to transform the data points at an optimal 94% movement from the original, unaligned position which is similar to solely constraining Z. This transformation therefore provides the optimal alignment accuracy. At the same time, the increased DoF constraints prevent the LR instrument location from moving from its original position within SA ensuring that when multiple instrument locations are implemented (when measuring large-scale wind turbine blades) further errors are removed.

The single B-Spline point alignment procedure also has a short inspection cycle-when using 32 points along the test piece B-Spline, the process is completed in less than 5 min.

Therefore, the single B-Spline point alignment with DoF constraints in *Z*, *Rx* and *Ry* provides blade manufacturers with a quick, simple and accurate aerofoil profile measurement procedure.

5.2. Double B-spline point alignment

Similarly to the single B-Spline point alignment, the results for double B-Spline points show that alignment performance is compromised as more DoF constraints are applied to the transformation procedure. However, the trends demonstrated in single B-Spline point alignment are not as prominent. The reason for this is that SA aligns each of the two B-Splines in unison when transforming with just rotational DoF (*Rx*, *Rz* and *Rz*). This imposes additional constraints onto the transformation, removing the notional movement of the LR instrument in SA but also lowering the ability for points to be transformed (generating a lower TMP than single B-Spline point alignment).

With less favourable trends, optimal DoF combinations vary between different test piece Rx, Ry and Rz positions (Experiment 3.1, 3.2, 3.3 and 3.4). This inconsistency prevents the establishment of a single best procedure for double B-Spline alignment. With two B-Splines to measure, the procedure also has an inspection time twice as long as single B-Spline measurement. Nonetheless, whilst the Double B-Spline point alignment with DoF constraints in either Z or X and Z still provides a relatively quick and simple procedure, it does not provide confidence that the measurement accuracy is optimised for each measurement.

When reducing the separation distance between B-Splines, the results from Experiment 4 show slight improvements in alignment accuracy (and the TMP confirms this) but the optimal DoF combination inconsistencies remain.

5.3. Single B-spline to double B-spline comparison.

Comparing these procedures, the optimal DoF combinations raw data, shown in Figs. 14 and 15, have similar performing alignment accuracies. However, the largest difference between the methods is in the variation in best ranked solutions.

The single B-Spline point alignment experiment shows constrained Z, Rx and Ry DoF as the top performing alignment for each variation of simulated blade sag and twist, whilst the double B-Spline method's optimal DoF combinations change for different alignment requirements. The consistency of the single B-Spline point alignment method therefore gives blade manufacturers more confidence that this measurement method is orientating data points in an accurate representation of the inspected blade aerofoil profile.

Also, the single B-Spline point alignment provides results in less time than the double B-Spline method, confirming the superiority of the single B-Spline method.

5.4. Complete blade inspection viability

The single B-Spline method inspects a small segment of a blade, treating it as an independent alignment assessment in order to account for any flex within the total blade. Replicating this process

at one metre intervals along each face of the blade would enable a complete inspection picture to be generated.

The results from Experiment 1 show that the distance of inspection from the root of the blade has no effect on alignment capabilities. Therefore, this method can be implemented successfully to generate high accuracy total blade inspection.

5.5. Experiment evaluation and recommendations

The procedure and software used in this investigation rely on surface features, such as variation is surface topography, to aid measurement alignment. This causes measured objects with complex shapes and surfaces to have the potential for improved data point alignment accuracy above simple objects with few features.

The experiments reported use a simple, constant radius curved test piece to simulate the complex, multi-featured curvature of a wind turbine blade. This caused the experimental alignment accuracies to be compromised, with optimal alignment only to within a mean of 5mm of the required measured point. The next stage of investigations should therefore use a more complex test piece, which replicates a blade segment, in order to remove this error and uncertainty. Carrying this out would increase the TMP further and enable smaller Point-to-Point distances; improving the overall alignment accuracy values. This further investigation is required to verify this paper's findings. Finally the results would be validated with data collected from actual wind turbine blade inspection in a factory in order to provide a quantitative value for LR measurement accuracy.

6. Conclusion

The use of LR for constrained Z, Rx and Ry DoF single B-Spline point alignment is presented in this paper. This procedure uses SA to eradicate the error introduced into large-scale wind turbine blade inspection by chordwise and spanwise flexing.

The LR enables accurate and fast, non-contact measurement whilst the experimental procedure proposed ensures measured data point to CAD model alignment is optimised in a simple and adaptable manner.

Experimental results show that the single B-Spline method is capable of enhancing wind turbine blade inspection reliability, thus providing blade manufacturers with confidence that their product is of accurate aerofoil profile. The study has also found no benefits are derived from using the double B-Spline method.

There is also potential for the technique to be developed for use in the inspection of other large, non-rigid structures that require high dimensional accuracy for their operational effectiveness. These could include aircraft fuselage and wings, large solar panels, radar and telescope dishes and possibly large space structures.

Acknowledgement

This research is part of the wind turbine structural condition monitoring program funded by EPSRC through the Centre for Through Life Engineering Services (EP/1033246/1, Project SC006) and EPSRC Impact Acceleration Award.

References

[1] J. Talbot, Q. Wang, N. Brady, R. Holden, Offshore wind turbine blades measurement using coherent laser radar, Measurement 79 (2016) 53–65.
[2] G.N. Peggs, et al., Recent developments in large-scale dimensional metrology, Proc. Inst. Mech. Eng. Part B: J. Eng. Manuf. 223 (B6) (2008) 571–595.
[3] W.T. Estler, K.L. Edmundson, G.N. Peggs, D.H. Parker, Large-scale metrology – an update, CIRP Ann. – Manuf. Technol. 51 (2) (2002) 587–609.
[4] F. Franceschini, M. Galetto, D. Maisano, L. Mastrogiacomo, Large-scale dimensional metrology (LSDM) from tapes and theodolites to multi-sensor systems, Int. J. Precis. Eng. Manuf. 15 (8) (2014) 1739–1758.
[5] Y.H. Li, Y.R. Qiu, Y.X. Chen, K.S. Guan, A novel orientation and position measuring system for large and medium scale precision assembly, Opt. Lasers Eng. 62 (2014) 31–37.
[6] A. Fischer, S. Park, 3D scanning and level of detail modelling for design and manufacturing, CIRP Ann. Manuf. Technol. 47 (1) (1998) 91–94.
[7] Y. Chu, J. Gou, H. Wu, Z. Li, Localization algorithms: performance evaluation and reliability analysis, IEEE Int. Conf. Robot. Autom. (1998) 3652.
[8] O. Bottema, B. Roth, Theoretical Kinematics, New York, Dover, 1990, ch.1.
[9] P. Besl, N. Mckay, A method for registration of 3-D shapes, IEEE 14 (2) (1992) 239–256.
[10] S. Rusinkiewicz, M. Levoy, Efficient variants of the ICP algorithm, IEEE (2011) 145.
[11] C. Yunyong, Z. Dinghua, H. Shengli, B. Kun, Research on a weighting alignment method for investment casting turbine blade shape inspection, Technol. Innov. Conference 2009 (ITIC 2009), International (2009) 1–4.
[12] A. Jaramillo, P. Boulanger, F. Prieto, On-line 3-D inspection of deformable parts using FEM trained radial basis functions, In: Proceedings of the IEEE 12th International Conference on Computer Vision Workshops (ICCV Workshops), pp.1733–1739, Sept. 27 2009–Oct. 4 2009.
[13] Quality Digest, Metris Metrology, Laser Radar supports Engineering of wind turbine blade aerodynamics, 2009. Available: ⟨http://www.qualitydigest.com/inside/twitter-ed/laser-radar-supports-engineering-wind-turbine-blade-aerodynamics.html⟩.
[14] Y. Zhang, Basic kinematics of constrained rigid bodies, Introduction to Mechanism, ch.4, Carnegie Mellon University.
[15] K. Lee, H. Woo, T. Suk, Data reduction methods for reverse engineering, Int. J. Adv. Manuf. Technol. 17 (10) (2001) 735–743.
[16] S. Lee, D. Chang, A laser sensor with multiple detectors for freeform surface digitization, Int. J. Adv. Manuf. Technol. 31 (5–6) (2006) 474–482.
[17] H. Fu, L. Ju, X. Li, The digital and high-precision error detection of complex freeform surface, In: Proceedings of the 9th International Conference on Computer-Aided Industrial Design and Conceptual Design, CAID/CD, pp. 646-651, 2008.
[18] T. Slotwinski, P. Blanckaert, Frequency modulated coherent laser radar technology, In: Proceedings of 3rd Workshop on Optical Measurement Techniques, OPTIMES, Optical Measurement Technologies for Structures and Systems, 386–391, 2007.
[19] J.H. Burge, P. Su, C. Zhao, T. Zobrist, Use of a commercial laser tracker for optical alignment, Opt. Syst. Align. Tolerancing 6676 (2007).
[20] Quality Digest, D. White, Coherent Laser Radar: true non-contact 3-D measurement has arrived, 1999. Available: ⟨http://www.qualitydigest.com/aug99/html/body_radar.html⟩.
[21] Quality Digest, Study: Comparison between Photogrammetry and Laser Radar, 2010. Available: ⟨http://www.qualitydigest.com/inside/cmsc-article/study-comparison-between-photogrammetry-and-laser-radar.html#⟩.
[22] S. Jecić, N. Drvar, The assessment of structured light and laser scanning methods in 3D shape measurements. In: Proceedings of the 4th International Congress of Croatian Society of Mechanics, 237-244, 2003.
[23] Nikon Metrology UK, Laser Radar Training Notes For LR Driver 5.0 and Spatial Analyser, 2010.
[25] New River Kinematics, SpatialAnalyzer®: Features & Benefits, 2014. Available: ⟨http://www.kinematics.com/spatialanalyzer/features.php⟩.
[26] New River Kinematics, SpatialAnalyzer®: Unified Spatial Metrology Network (USMN), 2014. Available: ⟨http://www.kinematics.com/spatialanalyzer/usmn.php⟩.
[27] Q. Wang, N. Zissler, R. Holden, Evaluate error sources and uncertainty in large scale measurement systems, Robot. Comput. Integr. Manuf. 29 (1) (2013) 1–11.
[28] ISO/TS 14253-3:2002. Geometrical product specifications (GPS) – inspection by measurement of work pieces and measuring equipment – Part 3: guidelines for achieving agreements on measurement uncertainty statements. International Organisation for Standardization; 2002.
[29] ISO 1101. Geometrical product specification (GPS) – Geometrical tolerancing-tolerances of form, orientation, location and run-out. International Organisation for Standardization; 2004.
[30] M. Galetto, L. Mastrogiacomo, D. Maisano, F. Franceschini, Cooperative fusion of distributed multi-sensor LVM (Large Volume Metrology) systems, CIRP Ann. – Manuf. Technol. 64 (2015) 483–486.
[31] Gurit, Wind turbine blade structural engineering, Wind Energy Handbook 3–Structural Design, 2015 ⟨http://gurit.fangle.co.uk/files/documents/3_Blade_Structure.pdf⟩.
[32] M.A. Homel, Blade Geometry and Solid Models, 2005. Available: ⟨http://www.mech.utah.edu/senior_design/05/index.php/WindTurbine/MikeGroupReport⟩.
[33] C. De Boor, On calculating with B-Splines, J. Approximation Theory 6 (1972) 50–62.
[34] G. Kumar, P. Kalra, S. Dhande, Parameter optimization for B-Spline curve fitting using genetic algorithms, The 2003 Congress on Evolutionary Computation, vol. 3, pp.1871–1878, 2003.
[35] C. De Boor, A Practical Guide to Spline, 27, Springer, 2001.